scientific reports

Check for updates

OPEN

Exactly solving the Kitaev chain and generating Majorana-zero-modes out of noisy qubits

Marko J. Rančić

Majorana-zero-modes (MZMs) were predicted to exist as edge states of a physical system called the Kitaev chain. MZMs should host particles that are their own antiparticles and could be used as a basis for a qubit which is robust-to-noise. However, all attempts to prove their existence gave inconclusive results. Here, the Kitaev chain is exactly solved with a quantum computing methodology and properties of MZMs are probed by generating eigenstates of the Kitev Hamiltonian on 3 noisy qubits of a publicly available quantum computer. After an ontological elaboration I show that two eigenstates of the Kitaev Hamiltonian exhibit eight signatures attributed to MZMs. The results presented here are a most comprehensive set of validations of MZMs ever conducted in an actual physical system. Furthermore, the findings of this manuscript are easily reproducible for any user of publicly available quantum computers, solving another important problem of research with MZMs—the result reproducibility crisis.

A Majorana fermion is its own antiparticle. This concept originally proposed in the context of particle physics more than 80 years ago experienced a rebirth with the work of Alexei Kitaev in early 2000s[1]. Kitaev proposed a toy model composed out of a chain of spinless fermions which are coupled by tunnelling t in the presence of p-wave superconducting pairing Δ and tunable chemical potential μ. A Kitaev chain has an exceptional feature that at low chemical potential and when tunnelling is comparable to the superconducting pairing exact zero energy solutions localised at the edges exist. Such states are immune to any small changes in local parameters and could potentially serve as a basis for a topological qubit[1–6].

Thus far, two common ways of getting a theoretical insight into the physics of Kitaev Hamiltonians in a broad range of parameters existed: numerical diagonalization of the many-body Hamiltonian and single-particle picture theories, such as diagonalizing the non-interacting Bogoliubov–de Gennes Hamiltonian. Numerical diagonalization of the many-body Hamiltonian is practically unfeasible for longer chains as the Hilbert space has 2^n states, where n is the number of sites in the chain. On the other hand, the Bogoliubov–de Gennes Hamiltonian operates on a Hilbert space of $2n$ states and has two zero energy solutions in the topological regime at low chemical potential. However, this Hamiltonian is a single-particle one and solves the Kitaev chain in a mean-field flavour. The reader should also be referred to studies with Matrix-product states[7] and Quantum Monte Carlo[8].

Many theoretical proposals and experimental validations showing Majorana-like features followed after Kitaev's work[9–22]. Some of the works received broad attention from the scientific community such as the spin-orbit nanowire in the presence of an external magnetic field and proximitized superconductivity[23] and deposited iron atoms on top of a superconductor[24]. Nevertheless, all of these experimental validations were followed by theory or experiments of topologically trivial phenomena mimicking those of Majorana zero modes[25–39]. To date, the verification of of MZMs remains one of the most debated on topics in physics.

Noisy quantum computers of today represent versatile platforms for probing quantum properties of chemical systems[40], QED systems[41] and even exotic, previously not-realized, condensed matter states such as time crystals[42], just to name a few. This manuscript aims to connect the world of MZMs with quantum computers. Here, I will present a method of solving the Kitaev chain Hamiltonian exactly with a quantum computing methodology and use a quantum computer to prepare exact eigenstates of such a Hamiltonian in what is commonly refereed to as a topologically non-trivial regime. The Kitaev chain in this study is composed out of noisy qubits. One key question which the reader of this study might have is: are the Majorana-zero-modes (MZMs)

TotalEnergies, Tour Coupole La Défense, 2 Pl. Jean Millier, 92078 Paris, France. email: marko.rancic@totalenergies.com

"artificiality" created on a quantum computer within this study actual MZMs or a mere representation of MZMs on a quantum computer? Given that quantum computers prepare actual quantum–mechanical wavefunctions this question might be paraphrased as: if two wavefunctions are exactly the same do they describe the same physical reality? The question of the meaning of the wavefunction is almost as old of quantum mechanics itself as it was initially posed by Max Born Ref.[43]. Until recently the meaning of the wavefunction remained a somewhat disputed question with works of Refs.[44,45] providing the most complete answer to-date. The author of this manuscript is closest to the view of Colbeck and Renner that a 1-to-1 mapping between the wavefunction and reality exist with a prior assumption that measurement settings could be freely chosen Ref.[45]. To put it simply: the MZMs generated on a quantum computer would be as real as they would be in any realisation in a condensed matter setting under the assumption of a non-super-deterministic universe.

Recent studies with quantum computers have focused on a single trait of MZMs (predominantly braiding) at $\mu = 0$ and $t = \Delta$ with approximate methods to prepare the ground state such as the imaginary time evolution. Historically the idea to probe braiding of MZMs with quantum computers was originally proposed in the context of superconducting qubits in Ref.[46] and was realised with a photonic system in Ref.[47] and a superconducting system[48]. Novel works with qubits also focus on teleportation of MZMs[49] and entanglement entropy[50].

In contrast to the above-mentioned works here I will present a general methodology to exactly obtain the eigenstates of the Kitaev Hamiltonian on a quantum computer in a broad range of parameters μ, t and Δ. Instead on focusing solely on a handful of features indicative of MZMs, my robust framework allows me to simultaneously test a record number of prediction about MZMs in an actual physical system. Two eigenstates of a 3-site Kitaev chain will show eight distinct features of MZMs: (1) a robust to noise degeneracy with their ground states at low chemical potential, an important feature of MZMs as discussed in Ref.[51]; (2) upon visually comparing the measured spectrum with a classically obtained Bogoliubov-de-Gennes (BdG) single-particle spectrum of MZMs a striking similarity is observed, like predicted in Kitaev's original proposal[1]. This similarity is quantified by calculating a mean absolute error of the measured data with respect to the BdG predictions; (3) the states under study have a well defined parity as discussed in Ref.[3], with (4) parity switches at specific values of the chemical potential in striking accordance with single-particle theories of MZMs—a feature originally predicted in Ref.[52]; (5) A non-conserved particle number of MZMs states as elaborated in Ref.[53]; (6) a Majorana-edge correlation function which decays with the chemical potential. Although this feature was quantitatively predicted in the thermodynamic limit here due to a finite chain size I display only qualitative matching[7]; (7) a display that MZMs favour exclusively Majorana-edge pairing at low chemical potential and (8) nearest-neighbour pairing at large values of the chemical potential another feature predicted in Kitaev's original proposal[1].

The goal of this study is to go beyond showing a handful of indications of MZMs and present a large number (eight) of corroborating evidence in a single reproducible experiment. Furthermore, the findings of this manuscript are easily reproducible for any user of publicly available quantum computers, solving another important issue with MZMs—the reproducibility crisis[54]. This study focuses on a 3-site Kitaev chain for doing experiments on actual quantum computers and 4-site chains for simulating the results of noiseless quantum computers with Qiskit. The chain length in this study was limited by noise levels of quantum computers. Experiments with longer chains of up to 7 qubits were a focus of a followup study[55] performed together with researchers from IBM where error mitigation had to be applied to get results for longer chains because of the noise levels in contemporary quantum computers.

Methodology

Throughout this paper, I will display results obtained by executing code developed for a combination of IBM's Qiskit and Google's quantum AI Cirq. The key ingredient of the code is a method for exactly preparing eigenstates of quadratic Hamiltonians. Preparing eigenstates of quadratic Hamiltonians is equivalent to preparing Slater determinants. Such states are called fermionic Gaussian states, as explained in Ref.[56] and are implemented with Google Quantum AI's Cirq OpenFermion[57]. Fermionic Gaussian states cannot describe excited states of exactly degenerate Hamiltonians[58]. Such wavefunctions are denoted as $|\psi\rangle$. As extensive numerical testing of the Kitaev chain showed multiple degeneracies at $\mu = 0$, I come as close to zero as $\mu = 10^{-8}|t|$.

The full n-site Kitaev chain Hamiltonian is given by

$$H = \sum_{k=1,n} \mu_k c_k^\dagger c_k - \sum_{\langle kj \rangle} \left(t_{kj} c_k^\dagger c_j - \Delta_{kj} c_k^\dagger c_j^\dagger + H.c. \right). \tag{1}$$

Here, μ_k denotes the chemical potential at kth site, t_{kj} denotes the tunnel hopping between sites k and j, Δ_{kj} the superconducting pairing, c_k annihilates an electron at site k while $c_k^\dagger$ creates the electron at the same site, and H.c. stands for an Hermitian conjugation. Majorana zero modes exist as solutions of the Kitaev Hamiltonian around $\mu = 0$ and $\Delta = -t$. This can be seen when substituting $c_k^\dagger = (\gamma_{2k-1} + i\gamma_{2k})/2$ and $c_k = (\gamma_{2k-1} - i\gamma_{2k})/2$ into Eq. (1), where γ_k is kth Majorana operator with the property $\gamma_k = \gamma_k^\dagger$. Throughout this paper, I will assume no local variations of these variables on different sites, hence μ_k, t_{kj} and Δ_{kj} become μ, t and Δ.

I will calculate and measure expectation values of a number of observables, the expectation value of energy $E = \langle\psi|H|\psi\rangle$, Majorana edge correlation function $\langle\psi|i\gamma_1\gamma_{2n}|\psi\rangle$[7] (where n denotes the number of sites and i denotes a complex number), Majorana site correlation function $\langle\psi|i\gamma_1\gamma_k|\psi\rangle$, Majorana parity operator $\langle\mathcal{P}\rangle = \langle\psi|\prod_{k=1}^{n}\left(1 - 2c_k^\dagger c_k\right)|\psi\rangle$ and particle number operator $\langle N\rangle = \langle\psi|\sum_{k=1,n} c_k^\dagger c_k|\psi\rangle$. All of these quantities are expressed via fermionic creation and annihilation operators and transformed into a qubit representation via a Jordan-Wigner transformation[59].

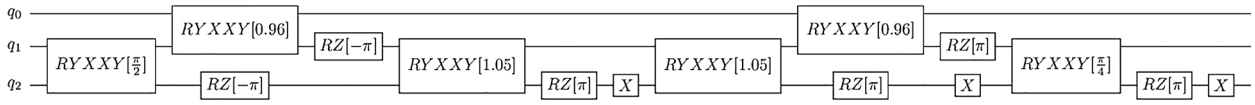

Figure 1. The circuit which generates a ground state of a 3 site Kitaev Hamiltonian at $t = -1, \Delta = 1$ and $\mu = 10^{-8}$. A general procedure for obtaining quantum computing circuits which represent the ground state of arbitrary quadratic Hamiltonians is given in Supplementary material Section S1.

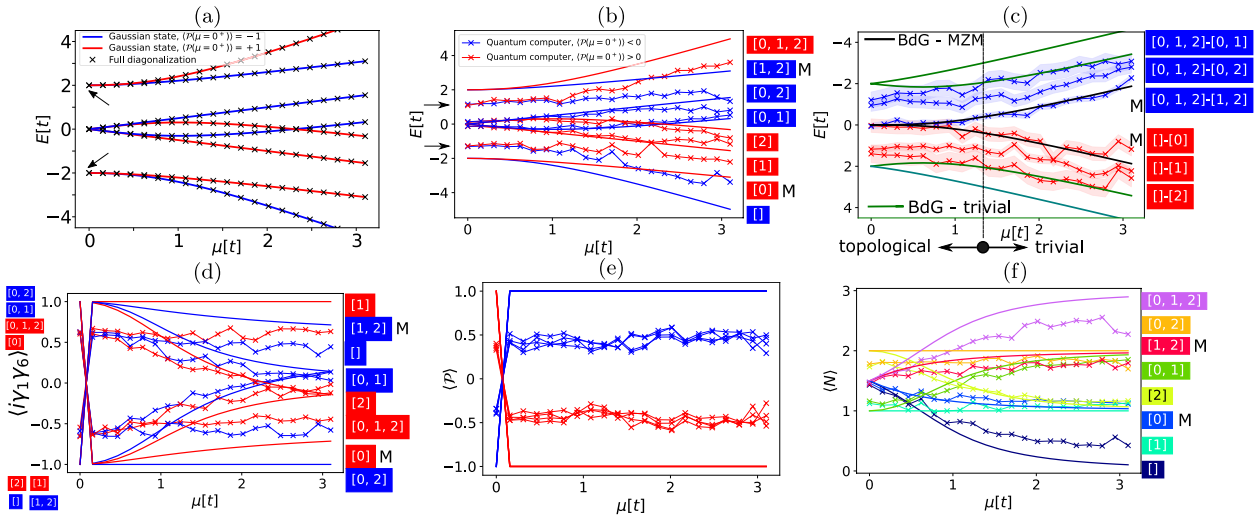

Figure 2. Quantities of the Kitaev Hamiltonian at $t = -1$ and $\Delta = 1$ as a function of the chemical potential μ in units of absolute value of tunnelling $[t]$. (**a**–**e**) Black "x" symbols represent a result of a numerical diagonalization on a classical computer. Red "x" symbols (full lines) values obtained on a quantum computer (ideal simulator of quantum computers) with $\langle P(\mu = 0^+)\rangle = 1$. Blue "x" symbols (full lines) values obtained on a quantum computer (ideal simulator of quantum computers) with $\langle P(\mu = 0^+)\rangle = -1$. The black arrows in (**a**,**b**) denote the position of the possible topological degeneracy. The "M" in (**b**,**c**,**d**,**f**) denotes the alleged MZM state. (**a**,**b**) The full spectrum of the Kitaev Hamiltonian obtained with Gaussian states compared to a numerical diagonalization (**a**) and IBMQ Santiago (**b**). (**c**) The single-particle picture BdG spectrum (full line) compared to the BdG spectrum on IBMQ Santiago. Shaded blue and red regions represent a root-mean-squared deviation of a given state with respect to a theoretical prediction of the BdG spectrum on QPUs in presence of pure-dephasing (see Supplementary section S3 for more details about the noise model). (**d**) Majorana edge-correlation function, an ideal simulation compared to the actual 3-site Kitaev chain composed out of qubits. (**e**) Parity—an ideal simulation compared to the actual 3-site Kitaev chain composed out of qubits. (**f**) Particle number on an ideal simulator (full lines) and actual 3-site Kitaev chain composed out of qubits (x-shaped coloured symbols).

According to Eq. (17) in Ref.[52], a topological state is supposed to exhibit parity switches at a chemical potential

$$\mu_{\mathrm{PS}} = \pm 2\sqrt{t^2 - \Delta^2}\cos\left(\frac{\pi p}{n+1}\right), \tag{2}$$

where $p = 1, \ldots, n/2$ for an even number of sites in the Kitaev chain n and $p = 1, \ldots, (n-1)/2$ for an odd n.

In Fig. 1 I display a quantum computer circuit for generating a ground state of a 3-site Kitaev Hamiltonian at $t = -1, \Delta = 1$ and $\mu = 0^+ = 10^{-8}$, denoted by [ ]. This circuit is composed from nearest-neighbour two-qubit gates defined by $RYXXY(\alpha) = \exp(-i(X \otimes Y - Y \otimes X)\alpha/2)$, and $RZ(\beta)$ gates (rotations of the qubit around the z-axis of the Bloch sphere for an angle β) and X gate rotates a qubit around the x-axis of the Bloch sphere for an angle of π. All excited energy eigenstates of the 3−site Kitaev Hamiltonian at the given parameter regime are built by first applying X gates to appropriate qubits and then executing the circuit in Fig. 1. For instance the first excited state is obtained by applying an X gate to qubit $q0$ followed by the execution of the circuit in Fig. 1 and is denoted as [0]. The highest energy state is obtained by applying X gates to qubits $q0$, $q1$, $q2$ followed by the execution of the circuit in Fig. 1, and is denoted as [0, 1, 2]. Google Quantum AI's Cirq calculates the optimal angles α and β based on the input of μ, Δ and t. A more detailed discussion on how such circuits are generated is given in Supplementary Material Section S1.

A comparison between theory and experiment

In Fig. 2a I display the spectrum of a 3-site Kitaev chain Hamiltonian having $2^n = 8$ eigenstates. Here, a comparison is given between a full diagonalization of the Kitaev Hamiltonian (black "x" symbols) and a solution obtained by implementing Gaussian states on an ideal quantum computer simulator (red and blue full lines). The red (blue) colour denotes states for which $\langle \mathcal{P}(\mu = 0^+) \rangle = +1(-1)$. Upon visual comparison these solutions show excellent agreement. The spectrum in subfigure (a) has a lowest energy state (highest energy state) with a next higher (lower) energy state degenerate to it around $\mu = 0$, and such degeneracies are marked with arrows. It should be noticed that there is a striking matching between a full numerical diagonalization and the fermionic Gaussian states.

In subfigure (b) I compare Gaussian states on an ideal simulator of quantum computers with their realisation on IBMQ Santiago. The circuit of the quantum eigenstate of the Kitaev chain is composed out of 6 two-qubit gates (*RYXXY* is implemented with two CNOT + single-qubit gates) and 9–13 single-qubit gates. The experiment is conducted for 8192 shots, with CNOT errors of 0.74% and readout errors of 1.5%. Single-qubit errors are not specified, however the average single-qubit frequency is 4.7 GHz with a pure dephasing time $T_2 = 70$ μs and qubit relaxation time $T_1 = 83\,\mu$s. Consequently, single-qubit gate errors influence the results much less than readout and two-qubit gate infidelity. Although all eigenstates move towards zero energy due to quantum noise, the degeneracy between states [ ] and [0] is not lifted by quantum noise. Similarly to that, the degeneracy between states [1, 2] and [0, 1, 2] follows the same pattern. One possible explanation for this degeneracy would be that it is topological in nature which would be the case if states [0] and [1, 2] are indeed Majorana zero modes.

The BdG Hamiltonian solves the problem of the Kitaev chain in a single-particle picture. It features electrons and holes and their energy splitting from their ground state (that of electrons and that of holes). Even though the Kitaev chain is rather short, the BdG Hamiltonian (subfigure (c)) is indicating the presence of two zero energy eigenstates (zero in the context of how far away are they from their respective groundstate) which split in energy as the chemical potential μ is varied. This robust feature exist both in theory and on a noisy quantum computer. The BdG Hamiltonian has $2n = 6$ eigenstates for a 3-site Kitaev chain. For the alleged MZM states, the BdG energy is in remarkable visual accordance with the measured output of the quantum device. One can quantify this by defining a mean absolute error as $\mathrm{ME} = \left(\sum_i |\mathrm{x_i} - \mathrm{y_i}|\right)/\mathrm{m}$, where m is the total number of measurements/predictions, x_i is the ith measurement of energy from the quantum device and y_i is the ith prediction of the BdG Hamiltonian. I find a $\mathrm{ME} = 0.129$ for $-1.87 \leq y_i \leq 1.87$. To further corroborate the correlation between the model and the data I have performed an estimation of the R^2 parameter with scipy.stats.linregress and obtained $0.95\,[0, 1, 2] - [1, 2]$ and 0.75 for $[] - [0]$ indicating a strong correlation between the model and measured data, even in the presence of quantum noise.

When $t = -\Delta$ an n-site Kitaev chain remains in the topological regime up to $\mu = 2t(1 - 1/n)$. In the case of $n = 3$ the system is in the topological regime up to $\mu = 4/3$—first 9 points in the subfigure (c) are topological. For an in-depth discussion on how this condition is calculated the reader is refereed to Supplementary Material Section S2. States which are split from zero energy at low μ are often referred to as topologically trivial states in literature. It should be noted that although Majorana zero modes remained at zero energy, the topologically trivial states are further shifted towards zero as compared to theory due to quantum noise at low μ. For a more quantitative analysis of the noise present in the system I revert the reader to Supplementary Material S3.

To further corroborate the Majorana zero mode nature of eigenstates of the Kitaev Hamiltonian I performed experiments and calculated the Majorana edge correlation function, $\langle i\gamma_1\gamma_6 \rangle$, where 1 and 6 are indices of the Majoranas on the edge of the Kitaev chain. If this number is $+1(-1)$ this would mean that the Majoranas on the edges are correlated(anti-correlated) and if this number is 0 there is no Majorana pairing in the system. In subfigure (d) we see that the states [0] and [1, 2] behave exactly as predicted by mean-field theory, as the chemical potential is varied the Majorana states at the edges of the chain become less (anti)-correlated. However, the experimental value does not reach ± 1 due to quantum noise. For a more quantitative analysis of the Majorana edge correlation function I revert the reader to Supplementary Material S4.

As further consistency checks, I performed measurements and simulations of the parity of the eigenstates of the Kitaev Hamiltonian, and these results are displayed in subfigure (e). The eigenstates are clearly separated in terms of parity ± 1 in case of theory, and positive and negative in case of experiment. A naive expectation for MZMs is that they do conserve parity as pairs of particles can be freely generated from the superconducting condensate. Similarly to energy measurements, the discrepancy between the theoretical and the experimental values is due to quantum noise. It should be noted that the eigenstates undergo a topological phase transition in which the parity of all eigenstates switches between the first two points ($\mu_1 = 10^{-8}$ and $\mu_2 = 0.155$). This topological phase transition is predicted to occur within the single-particle picture at $\mu = 0$ and will be discussed in detail later in this section.

Lastly in subfigure (f) I plot the total particle number of particles for different eigenstates. A naive expectation for MZMs is that they do not conserve particle number as a function of chemical potential, at least in a picture where the topological region is observed separately from the bare superconductor[53,60]. This is due to the fact that in the picture of a separated topological and non-topological condensate pairs of particles can be freely generated from the superconducting condensate[53], and states [0] and [1, 2] behave in the expected manner. If particle number was conserved (a good quantum number) this would mean that as the parameters of the Hamiltonian and respective eigenstate are changed, the expectation value of the particle number operator would remain the same. For states [0] and [1, 2] the particle number is not conserved at small μ and then saturates to a value 1 or 2 at large values of μ.

In Fig. 3 I test the single-particle prediction that parity switches occur according to Eq. (2). Tunnelling is kept constant at $t = -1$, $\Delta = 0.25, 0.5, 0.75, 1, 1.25$ and μ is varied between 10^{-8} and 3.1 in 20 increments of 0.155. The points where parity switches represent a topological phase transition. Squared markers are added to ideal

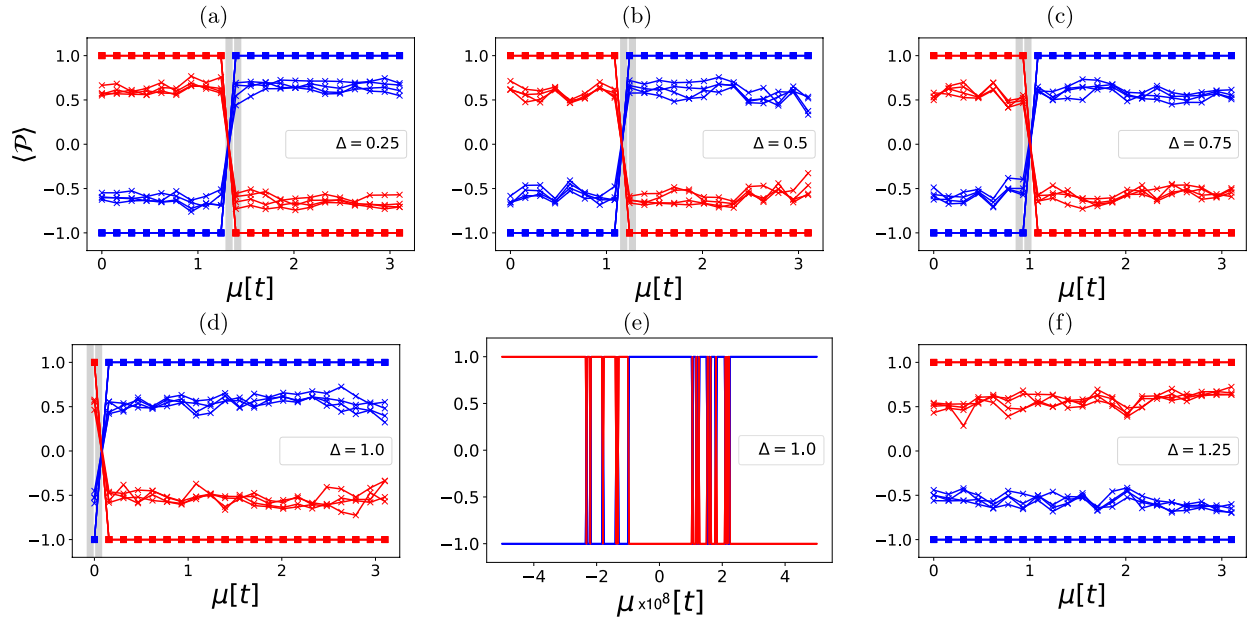

Figure 3. (**a**–**d**) and (**f**) Parity switches at $t = -1$ for different values of Δ and for 20 values of μ between 10^{-8} and 3.1 with a 0.155 increment. (**e**) Parity switches for 400 values of μ between -5×10^{-8} and 5×10^{-8}.

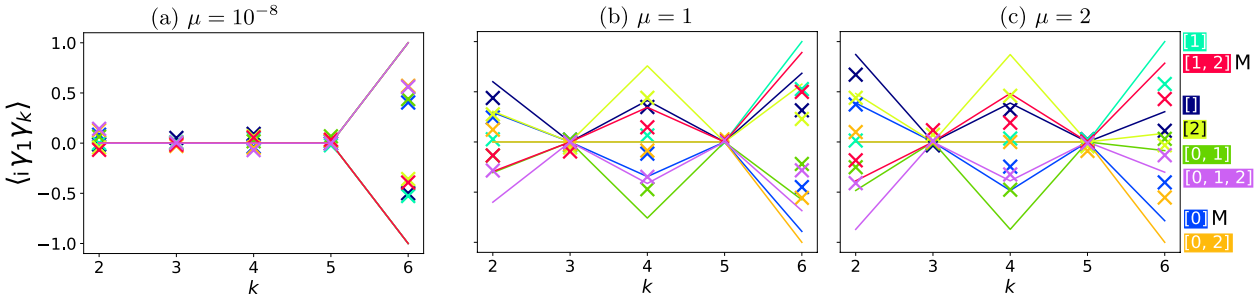

Figure 4. Site correlation function where k denotes the site at different values of the chemical potential in the topological regime $\Delta = -t = 1$. Full lines denote values obtained by an ideal simulator of quantum computers at points of integer k and "x"-markers are output from IBMQ Santiago. Colour code is explained on the right.

quantum simulator data. The grey line represents a region where the parity switching is likely to occur and it exists due to a limited resolution in μ in which the experiment is performed. The white line is the exact expected position of such a transition as predicted by the single-particle picture. Such parity switches could be understood as points in which two MZM eigenstates cross the zero of energy.

The results show that the behaviour of the exact solutions and the experiment is much in line with the prediction: parity switches occur exactly where they are predicted with Eq. (2). Here, I find the only minor discrepancy between the single-particle picture and the full solution—parity switches occur in a narrow parameter region in μ (see subfigure (e)) and not in a single point. However, this region in parameter space of μ is quite narrow—on the order of 4×10^{-8} that I conclude that it is quite in line with predictions. A comparison between the simulated results (squares) and outputs of the quantum computers ("x" markers) show that this feature is quite robust to quantum noise. Although the value of the parity decreases on quantum computers as compared to ideal simulations, the point where parity switches is robust to any relaxation and pure dephasing. This an indication that this parity switches represent a topological phase transition.

In Fig. 4 we observe the Majorana site correlation function $\langle i\gamma_1\gamma_k \rangle$ in the topological regime $\Delta = -t = 1$ as a function of the chemical potential μ. First it should be noted that the operator $i\gamma_1\gamma_k$ is non-Hermitian at $k = 1$ so the site correlation operator is an observable only when $k > 1$.

At low chemical potential states [0] and [1, 2] are exhibiting a Majorana-like character—a Majorana site correlation function localized at edges which is ± 1 for the results of an ideal simulation (full lines). The actual execution on a quantum computer (colored "x" symbols) follows a similar qualitative trend but does not quantitatively reach ± 1 due to quantum noise. As the chemical potential increased, Majorana zero modes start favoring correlations between neighboring Majorana fermions more. This is potentially a key differentiation between MZMs and trivial zero-energy states such as Andreev bound states, as the latter are not localized at the edges[34].

This figure also allows the determination of the type of quantum noise dominating in the experiment. When observing the value of the site-correlation function for states [ ] and [0, 1, 2] at $\mu = 1$ and $\mu = 2$ around $k = 2$ we

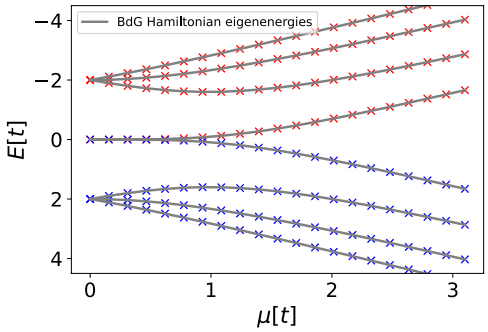

Figure 5. Quantities of a 4-site Kitaev Hamiltonian at $t = -1$ and $\Delta = 1$ as a function of the chemical potential μ in units of absolute value of tunnelling [t]. Red denotes values obtained on an ideal simulator of quantum computers with $\langle P(\mu = 0^+)\rangle = 1$. Blue denotes values obtained on an ideal simulator of quantum computers with $\langle P(\mu = 0^+)\rangle = -1$. The single-particle picture BdG spectrum, diagonalizatioin of the BdG Hamiltonian (grey lines) compared to Gaussian state solutions (coloured markers).

see that the state [0, 1, 2] and the state [ ] have the same absolute value in theory. However, in the experimental realization the measured value of the site correlation function is much closer to the theoretical value for the state [ ] as opposed to the state [0, 1, 2]. The only difference between these two states are the simulations three single qubit X gates applied to qubits $q0$, $q1$ and $q2$. It should be noted that single qubit gates by themselves should not have such a profound effect on state fidelity due to the fact that they are quite noise robust. This is a strong indication that qubit cross-talk is present and the dominating dephasing source in IBMQ Santiago—an effect already known and well characterized for other IBMQ processors such as IBMQ Poughkeepsie[61]. In Supplementary Material S5 I give another realization of the same experiment corroborating the same qualitative features. In Supplementary material S6 the same results are presented for a 4-site Kitaev chain on simulators of quantum computers. Example of a 4-site BdG spectrum is given here just to show that the methodology generalizes to longer chains Fig. 5.

Comparison with non-topological phenomena mimicking MZMs A number of topologically trivial phenomena mimic the behavior of MZMs in some regards. Caroli-de Gennes-Matricon (CdGM) states[37], Yu-Shiba-Rusinov (YSR) states[62] and Andreev bound states[34] are the most common ones refereed to in the literature. CdGM states are subgap states close to zero energy when $\Delta \ll \mu$. In our case the sticking of the energy levels to zero occurs in the opposite limit when $\Delta \gg \mu$. Furthermore, YSR states and Andreev bound states require a non-superconducting region. A bound state which is created in these two cases is local in nature[34]- unlike the case presented here no long-range Majorana correlations are present.

Conclusion

To conclude, here I solved the Kitaev chain exactly with quantum computing methods and showed both theoretically and experimentally that two eigenstates of the Kitaev Hamiltonian have a large number of features that corroborate their Majorana zero mode nature. They are zero energy excitations of their respective groundstate with a robust-to-noise degeneracy, they have a Majorana edge-correlation function which decays with the chemical potential. Furthermore, Majorana zero modes favour Majorana pairing between edges of the Kitaev chain, do not preserve particle number and have parity switches at points in the parameter space as predicted by single-particle theories. The results presented here are the most complete set of experimental validations which confirm the existence of Majorana zero modes on the edges of a Kitaev chain, as the eigenstates of the Kitaev Hamiltonian are tested for eight distinct indications of MZMs in a single, reproducible experiment.

Data availability

Full experimental data and code is available at 10.5281/zenodo.6323467.

Received: 20 July 2022; Accepted: 14 November 2022
Published online: 18 November 2022

References

1. Kitaev, A. Y. Unpaired Majorana fermions in quantum wires. *Phys. Uspekhi* **44**, 131 (2001).
2. Beenakker, C. Search for Majorana fermions in superconductors. *Annu. Rev. Condens. Matter Phys.* **4**, 113 (2013).
3. Sarma, S. D., Freedman, M. & Nayak, C. Majorana zero modes and topological quantum computation. *NPJ Quantum Inf.* **1**, 1 (2015).
4. Hu, Y., Cai, Z., Baranov, M. A. & Zoller, P. Majorana fermions in noisy Kitaev wires. *Phys. Rev. B* **92**, 165118 (2015).
5. Aseev, P. P., Klinovaja, J. & Loss, D. Lifetime of Majorana qubits in Rashba nanowires with nonuniform chemical potential. *Phys. Rev. B* **98**, 155414 (2018).
6. Mishmash, R. V., Bauer, B., von Oppen, F. & Alicea, J. Dephasing and leakage dynamics of noisy Majorana -based qubits: Topological versus Andreev. *Phys. Rev. B* **101**, 075404 (2020).
7. Miao, J.-J., Jin, H.-K., Zhang, F.-C. & Zhou, Y. Majorana zero modes and long range edge correlation in interacting Kitaev chains: Analytic solutions and density-matrix-renormalization-group study. *Sci. Rep.* **8**, 1 (2018).

8. Nasu, J. & Motome, Y. Spin dynamics in the Kitaev model with disorder: Quantum Monte Carlo study of dynamical spin structure factor, magnetic susceptibility, and NMR relaxation rate. *Phys. Rev. B* **104**, 035116 (2021).
9. Jiang, L. *et al.* Majorana fermions in equilibrium and in driven cold-atom quantum wires. *Phys. Rev. Lett.* **106**, 220402 (2011).
10. Wiedenmann, J. *et al.* 4π-periodic Josephson supercurrent in HGTE-based topological Josephson junctions. *Nat. Commun.* **7**, 1 (2016).
11. Fu, L. & Kane, C. L. Superconducting proximity effect and Majorana fermions at the surface of a topological insulator. *Phys. Rev. Lett.* **100**, 096407 (2008).
12. Deng, M. *et al.* Anomalous zero-bias conductance peak in a NB-INSB nanowire-NB hybrid device. *Nano Lett.* **12**, 6414 (2012).
13. Fu, L. & Kane, C. L. Josephson current and noise at a superconductor/quantum-spin-hall-insulator/superconductor junction. *Phys. Rev. B* **79**, 161408 (2009).
14. Rokhinson, L. P., Liu, X. & Furdyna, J. K. The fractional AC Josephson effect in a semiconductor-superconductor nanowire as a signature of Majorana particles. *Nat. Phys.* **8**, 795 (2012).
15. Sau, J. D. & Sarma, S. D. Realizing a robust practical Majorana chain in a quantum-dot-superconductor linear array. *Nat. Commun.* **3**, 1 (2012).
16. He, Q. L. *et al.* Chiral Majorana fermion modes in a quantum anomalous hall insulator-superconductor structure. *Science* **357**, 294 (2017).
17. Banerjee, A. *et al.* Proximate Kitaev quantum spin liquid behaviour in a honeycomb magnet. *Nat. Mater.* **15**, 733 (2016).
18. Wang, D. *et al.* Evidence for Majorana bound states in an iron-based superconductor. *Science* **362**, 333 (2018).
19. Manna, S. *et al.* Signature of a pair of Majorana zero modes in superconducting gold surface states. *Proc. Natl. Acad. Sci.* **117**, 8775 (2020).
20. Volpez, Y., Loss, D. & Klinovaja, J. Second-order topological superconductivity in π-junction Rashba layers. *Phys. Rev. Lett.* **122**, 126402 (2019).
21. Hoffman, S., *et al.* Majorana zero modes emulated in a magnetic molecule chain. arXiv:2110.12019 (arXiv preprint) (2021).
22. Díaz, S. A., Klinovaja, J., Loss, D. & Hoffman, S. Majorana bound states induced by antiferromagnetic skyrmion textures. *Phys. Rev. B* **104**, 214501 (2021).
23. Mourik, V. *et al.* Signatures of Majorana fermions in hybrid superconductor–semiconductor nanowire devices. *Science* **336**, 1003 (2012).
24. Nadj-Perge, S. *et al.* Observation of Majorana fermions in ferromagnetic atomic chains on a superconductor. *Science* **346**, 602 (2014).
25. Chiu, C.-K., Ghaemi, P. & Hughes, T. L. Stabilization of Majorana modes in magnetic vortices in the superconducting phase of topological insulators using topologically trivial bands. *Phys. Rev. Lett.* **109**, 237009 (2012).
26. Ruby, M., Heinrich, B. W., Peng, Y., von Oppen, F. & Franke, K. J. Exploring a proximity-coupled co chain on pb (110) as a possible Majorana platform. *Nano Lett.* **17**, 4473 (2017).
27. Liu, C.-X., Sau, J. D., Stanescu, T. D. & Das Sarma, S. Andreev bound states versus Majorana bound states in quantum dot-nanowire-superconductor hybrid structures: Trivial versus topological zero-bias conductance peaks. *Phys. Rev. B* **96**, 075161 (2017).
28. Liu, C.-X., Sau, J. D. & Das Sarma, S. Distinguishing topological Majorana bound states from trivial Andreev bound states: Proposed tests through differential tunneling conductance spectroscopy. *Phys. Rev. B* **97**, 214502 (2018).
29. Sau, J. D. & Brydon, P. M. R. Bound states of a ferromagnetic wire in a superconductor. *Phys. Rev. Lett.* **115**, 127003 (2015).
30. Lee, E. J. *et al.* Spin-resolved Andreev levels and parity crossings in hybrid superconductor–semiconductor nanostructures. *Nat. Nanotechnol.* **9**, 79 (2014).
31. Chen, J. *et al.* Ubiquitous non-Majorana zero-bias conductance peaks in nanowire devices. *Phys. Rev. Lett.* **123**, 107703 (2019).
32. Woods, B. D., Chen, J., Frolov, S. M. & Stanescu, T. D. Zero-energy pinning of topologically trivial bound states in multiband semiconductor-superconductor nanowires. *Phys. Rev. B* **100**, 125407 (2019).
33. Vuik, A., Nijholt, B., Akhmerov, A. & Wimmer, M. Reproducing topological properties with quasi-Majorana states. *SciPost Phys.* **7**, 061 (2019).
34. Prada, E. *et al.* From Andreev to Majorana bound states in hybrid superconductor-semiconductor nanowires. *Nat. Rev. Phys.* **2**, 575 (2020).
35. Kayyalha, M. *et al.* Absence of evidence for chiral Majorana modes in quantum anomalous hall-superconductor devices. *Science* **367**, 64 (2020).
36. Kim, H., Nagai, Y., Rózsa, L., Schreyer, D. & Wiesendanger, R. Anisotropic non-split zero-energy vortex bound states in a conventional superconductor. arXiv:2105.01354 (arXiv preprint) (2021).
37. Chen, M. *et al.* Discrete energy levels of caroli-de gennes-matricon states in quantum limit in fete 0.55 se 0.45. *Nat. Commun.* **9**, 1 (2018).
38. Jäck, B., Xie, Y. & Yazdani, A. Detecting and distinguishing Majorana zero modes with the scanning tunnelling microscope. *Nat. Rev. Phys.* **3**, 541 (2021).
39. Chatzopoulos, D. *et al.* Spatially dispersing Yu-Shiba-Rusinov states in the unconventional superconductor fete 0.55 se 0.45. *Nat. Commun.* **12**, 1 (2021).
40. Peruzzo, A. *et al.* A variational eigenvalue solver on a photonic quantum processor. *Nat. Commun.* **5**, 1 (2014).
41. Stetina, T. F., Ciavarella, A., Li, X. & Wiebe, N. Simulating effective qed on quantum computers. *Quantum* **6**, 622 (2022).
42. Ippoliti, M., Kechedzhi, K., Moessner, R., Sondhi, S. & Khemani, V. Many-body physics in the nisq era: Quantum programming a discrete time crystal. *PRX Quantum* **2**, 030346 (2021).
43. Born, M. Quantenmechanik der stoßvorgänge. *Z. Phys.* **38**, 803 (1926).
44. Pusey, M. F., Barrett, J. & Rudolph, T. On the reality of the quantum state. *Nat. Phys.* **8**, 475 (2012).
45. Colbeck, R. & Renner, R. Is a system's wave function in one-to-one correspondence with its elements of reality?. *Phys. Rev. Lett.* **108**, 150402 (2012).
46. You, J., Wang, Z., Zhang, W. & Nori, F. Encoding a qubit with Majorana modes in superconducting circuits. *Sci. Rep.* **4**, 1 (2014).
47. Xu, J.-S. *et al.* Simulating the exchange of Majorana zero modes with a photonic system. *Nat. Commun.* **7**, 1 (2016).
48. Stenger, J. P. T., Bronn, N. T., Egger, D. J. & Pekker, D. Simulating the dynamics of braiding of Majorana zero modes using an IBM quantum computer. *Phys. Rev. Res.* **3**, 033171 (2021).
49. Huang, H.-L. *et al.* Emulating quantum teleportation of a Majorana zero mode qubit. *Phys. Rev. Lett.* **126**, 090502 (2021).
50. Xiao, X., Freericks, J. & Kemper, A. Determining quantum phase diagrams of topological Kitaev-inspired models on nisq quantum hardware. *Quantum* **5**, 553 (2021).
51. Klassen, J. & Wen, X.-G. Topological degeneracy (Majorana zero-mode) and 1+ 1d fermionic topological order in a magnetic chain on superconductor via spontaneous symmetry breaking. *J. Phys. Condens. Matter* **27**, 405601 (2015).
52. Hegde, S., Shivamoggi, V., Vishveshwara, S. & Sen, D. Quench dynamics and parity blocking in Majorana wires. *New J. Phys.* **17**, 053036 (2015).
53. Lin, Y. & Leggett, A. J. Towards a particle-number conserving theory of Majorana zero modes in p+ ip superfluids. arXiv:1803.08003 (arXiv preprint) (2018).
54. Frolov, S. Quantum computing's reproducibility crisis: Majorana fermions (2021).
55. Sung, K. J., Rančić, M. J., Lanes, O. T. & Bronn, N. T. Preparing Majorana zero modes on a noisy quantum processor. arXiv:2206.00563 (arXiv preprint) (2022).

56. Jiang, Z., Sung, K. J., Kechedzhi, K., Smelyanskiy, V. N. & Boixo, S. Quantum algorithms to simulate many-body physics of correlated fermions. *Phys. Rev. Appl.* **9**, 044036 (2018).
57. McClean, J. R. *et al.* Openfermion: The electronic structure package for quantum computers. *Quantum Sci. Technol.* **5**, 034014 (2020).
58. Greplova, E. Quantum information with fermionic gaussian states (2013).
59. Tranter, A., Love, P. J., Mintert, F. & Coveney, P. V. A comparison of the Bravyi–Kitaev and Jordan–Wigner transformations for the quantum simulation of quantum chemistry. *J. Chem. Theory Comput.* **14**, 5617 (2018).
60. Lapa, M. F. & Levin, M. Rigorous results on topological superconductivity with particle number conservation. *Phys. Rev. Lett.* **124**, 257002 (2020).
61. Murali, P., McKay, D. C., Martonosi, M., & Javadi-Abhari, A. Software mitigation of crosstalk on noisy intermediate-scale quantum computers, in *Proceedings of the Twenty-Fifth International Conference on Architectural Support for Programming Languages and Operating Systems*, pp. 1001–1016 (2020).
62. Balatsky, A. V., Vekhter, I. & Zhu, J.-X. Impurity-induced states in conventional and unconventional superconductors. *Rev. Mod. Phys.* **78**, 373 (2006).

Acknowledgements

I would like to thank endlessly A. Lj. Rančić for all her patience, support and science discussions during the course of this work. I am also grateful to O. Dmytruk for live discussions and explanations.

Author contributions

M.R. devised and conducted the entire study himself.

Competing interests

The author declares no competing interests.

Additional information

Supplementary Information The online version contains supplementary material available at https://doi.org/10.1038/s41598-022-24341-z.

Correspondence and requests for materials should be addressed to M.J.R.

Reprints and permissions information is available at www.nature.com/reprints.

Publisher's note Springer Nature remains neutral with regard to jurisdictional claims in published maps and institutional affiliations.